Development 134, 2981-2989 (2007) doi:10.1242/dev.007567

# Hox patterning of the vertebrate rib cage

**Daniel C. McIntyre[1], Sabita Rakshit[1], Alisha R. Yallowitz[2], Luke Loken[1], Lucie Jeannotte[3], Mario R. Capecchi[4] and Deneen M. Wellik[1,*]**

Unlike the rest of the axial skeleton, which develops solely from somitic mesoderm, patterning of the rib cage is complicated by its derivation from two distinct tissues. The thoracic skeleton is derived from both somitic mesoderm, which forms the vertebral bodies and ribs, and from lateral plate mesoderm, which forms the sternum. By generating mouse mutants in *Hox5*, *Hox6* and *Hox9* paralogous group genes, along with a dissection of the *Hox10* and *Hox11* group mutants, several important conclusions regarding the nature of the 'Hox code' in rib cage and axial skeleton development are revealed. First, axial patterning is consistently coded by the unique and redundant functions of Hox paralogous groups throughout the axial skeleton. Loss of paralogous function leads to anterior homeotic transformations of colinear regions throughout the somite-derived axial skeleton. In the thoracic region, Hox genes pattern the lateral plate-derived sternum in a non-colinear manner, independent from the patterning of the somite-derived vertebrae and vertebral ribs. Finally, between adjacent sets of paralogous mutants, the regions of vertebral phenotypes overlap considerably; however, each paralogous group imparts unique morphologies within these regions. In all cases examined, the next-most posterior Hox paralogous group does not prevent the function of the more-anterior Hox group in axial patterning. Thus, the 'Hox code' in somitic mesoderm is the result of the distinct, graded effects of two or more Hox paralogous groups functioning in any anteroposterior location.

**KEY WORDS: Hox code, Anteroposterior (AP) patterning, Developmental genetics, Posterior prevalence, Vertebral column, Primaxial/abaxial**

## INTRODUCTION

Differences in the anteroposterior (AP) patterning of the axial skeleton result in an enormous diversity of body plans in vertebrates. Hox genes were first described in *Drosophila* for their ability to cause segmental homeotic transformations of the body plan (Lewis, 1963; Lewis, 1978), and have since been found to be conserved throughout vertebrate evolution, suggesting their importance in patterning the vertebrate body plan. Whereas flies have eight Hox genes located in a single cluster, mammals have 39 Hox genes arranged in four clusters, which are further subdivided into thirteen paralogous groups based on sequence similarity and position within the cluster.

Hox expression along the vertebrate AP axis exhibits overlapping expression domains with unique and increasingly posterior limits of expression (Colberg-Poley et al., 1985; Duboule and Dolle, 1989; Izpisua-Belmonte et al., 1991). As a result of this colinear expression, more-posterior axial regions initially express greater numbers of Hox genes. The existence of a vertebrate 'Hox code' was proposed that would assign morphologies to each vertebra as a result of the combination of the Hox genes functioning in each region (Gruss and Kessel, 1991; Kessel and Gruss, 1990; Kessel and Gruss, 1991). Based on several studies, including early work on changes in Hox expression in the retinoic acid-treated limb, ectopic expression of mammalian Hox genes in *Drosophila*, and early genetic experiments which showed that loss-of-function of single Hox genes generally resulted in changes in only the vertebra at the anterior-most limit of expression, the model of 'posterior prevalence' has been put forth, which holds that posteriorly expressed Hox genes are functionally dominant over more anteriorly expressed genes (Bachiller et al., 1994; Duboule, 1991; Duboule and Morata, 1994; Kmita and Duboule, 2003).

A number of studies have shown that functional redundancy has been retained among Hox paralogous genes (Chen and Capecchi, 1997; Chen and Capecchi, 1999; Chen et al., 1998; Davis et al., 1995; Greer et al., 2000; Horan et al., 1995; Patterson et al., 2001; Rossel and Capecchi, 1999; Wahba et al., 2001; Wellik and Capecchi, 2003; Wellik et al., 2002). Horan et al. showed that whereas single mutants for *Hoxa4*, *Hoxb4* and *Hoxd4* resulted in incompletely penetrant phenotypes in the second or third cervical vertebra, loss-of-function of three of the four *Hox4* genes caused extensive cervical transformations, with C2 through C5 transformed towards a C1 phenotype (Horan et al., 1995). Complete removal of paralogous function of the *Hox10* and *Hox11* group genes has also been reported. These mutants display regional anterior homeotic transformations of the posterior axial skeleton (Wellik and Capecchi, 2003). Loss of *Hox10* paralogous function results in conversion of the entire lumbosacral region to a thoracic-like morphology. When the *Hox11* paralogous genes are removed, the entire sacral region undergoes transformation to a lumbar-like morphology.

Hox function in the thoracic region, however, has not been as clearly defined. First, both anterior and posterior homeotic transformations have been reported in this region for single Hox mutant animals. Single mutants in *Hox5* and *Hox6* paralogous groups have both resulted in phenotypes at the cervicothoracic transition. Whereas mutants for *Hoxa5* and *Hoxa6* both exhibit an ectopic rib at C7, constituting a posterior homeotic transformation, single mutants of *Hoxb5*, *Hoxb6* and *Hoxc6* demonstrate partially penetrant loss of rib formation at T1, constituting an anterior homeotic transformation (Garcia-Gasca and Spyropoulos, 2000; Jeannotte et al., 1993; Kostic

[1]Division of Molecular Medicine and Genetics, Department of Internal Medicine, [2]Department of Cellular and Developmental Biology, University of Michigan Medical Center, 109 Zina Pitcher, Ann Arbor, MI 48109-2200, USA. [3]Centre de Recherche en Cancérologie de l'Université Laval, Centre Hospitalier Universitaire de Québec, Québec, G1R 2J6, Canada. [4]Department of Human Genetics, University of Utah, and Howard Hughes Medical Institute, Salt Lake City, UT 84112, USA.

*Author for correspondence (e-mail: dwellik@umich.edu)

**Accepted 12 June 2007**

and Capecchi, 1994; Rancourt et al., 1995). As C7 and T1 are affected in both the *Hox5* and the *Hox6* single mutants, colinearity is not immediately apparent for these genes; however, paralogous mutants have not been examined for these groups. Mutants in the *Hox7*, *Hox8* and *Hox9* genes have also been examined (Chen and Capecchi, 1997; Chen et al., 1998; van den Akker et al., 2001). The reported defects in these mutants also show no clear colinearity. The phenotypes in these animals are reported to localize at both cervicothoracic and at thoracolumbar transition points, not to distinct AP regions of the axial skeleton. These combined results suggest that there are alternative mechanisms by which Hox genes govern patterning of the thoracic region.

Part of the difficulty in understanding patterning of the rib cage results from the nature of development of the thoracic skeleton. The thoracic vertebrae have a primaxial component that is derived from somitic mesoderm like the rest of the axial skeleton. This includes the axial vertebral elements as well as the proximal ribs. Unlike the rest of the axial skeleton, however, the thoracic skeleton also has an abaxial component – the sternum and sternal ribs, which are derived from the lateral plate mesoderm (Burke and Nowicki, 2003; Nowicki and Burke, 2000; Nowicki et al., 2003). Thus, the phenotypes in the thoracic region must be interpreted with respect to the distinct derivation of the tissues that comprise this portion of the axial skeleton.

In order to more completely understand how Hox genes pattern the vertebrate axial skeleton, including the rib cage, we have generated triple paralogous mutants in the *Hox5* and *Hox6* group genes as well as quadruple paralogous mutants in the *Hox9* group genes and characterized their phenotypes in the axial skeleton. We have also examined and compared the complete axial phenotype of the *Hox10* triple mutants and the *Hox11* triple mutants with the newly generated paralogous mutant groups. Each set of the paralogous mutants demonstrates functional redundancy in axial patterning and *Hox5*, *Hox6* and *Hox9* paralogous mutants display dramatic effects on rib cage morphology. Anterior homeotic transformations occur in distinct AP domains in the somite-derived primaxial skeleton for each set of paralogous mutants and these defects demonstrate clear colinearity. Although the AP boundaries of the vertebral transformations for each adjacent set of paralogous mutants overlap considerably, each paralogous mutant group imparts unique morphologies to the overlapping regions. Thus, the simplest interpretation of posterior prevalence in which the next-most posterior Hox group is functionally dominant over the more-anterior group is not supported by these results. Further, the lateral plate-derived abaxial phenotypes in these mutants overlap almost completely and these phenotypes are not colinear, suggesting an independent role for Hox genes in patterning the lateral plate-derived axial skeleton.

## MATERIALS AND METHODS

### Generation of mouse mutants

Mice mutant in the *Hox5*, *Hox6* and *Hox9* paralogous colonies were generated using standard genetic crosses (Boulet and Capecchi, 1996; Chen and Capecchi, 1997; Chen and Capecchi, 1999; Garcia-Gasca and Spyropoulos, 2000; Jeannotte et al., 1993; Kostic and Capecchi, 1994; Rancourt et al., 1995). Skeletal preparations were performed on E18.5 embryos throughout the study. *Hox10* and *Hox11* mutants were generated as described previously (Wellik and Capecchi, 2003).

### Skeletal phenotyping

Mouse embryos were skinned and eviscerated, fixed for 4 days in 95% ethanol, and prepared by alkaline digestion before staining with Alcian Blue 8GX for cartilage and Alizarin Red S for ossified bone. Embryos were then dissected and photographed in 97% glycerol (Wellik and Capecchi, 2003).

### Genotyping

Embryos were genotyped by PCR and the results analyzed on agarose gels. For *Hox5*, *Hox6* and *Hox9* paralogous genes, analyses were conducted using 12.5 μl reactions with the following conditions: 32 cycles of 94°C for 30 seconds, 64°C for 30 seconds, and 72°C for 30 seconds. The following primers were used for genotyping (F, forward; Rwt, wild-type reverse; Rmut, mutant reverse):

*Hoxa5*, 5′-ACTGGGAGGGCAGTGCCCCCACTTAGGACA-3′ (F) and 5′-CTGCCGCGGCCATACTCATGCTTTTCAGCT-3′ (Rwt) and 5′-GGCTACCTGCCCATTCGACCACCAAGCGAA-3′ (Rmut);

*Hoxb5*, 5′-TATGGCAGTGGCAGCTCTCTGAGCG-3′ (F) and 5′-CGAGGAGCGGTTGACGCTGAGATCCAT-3′ (Rwt) and 5′-CGTGTTCGAATTCGCCAATGACAAGAC-3′ (Rmut);

*Hoxc5*, 5′-CAACAACTTGTGTCTCAACGAGAGACAG-3′ (F) and 5′-GGAGAAGGGGTTACAGTCAGTCT-3′ (Rwt) and 5′-CGTGTTCGAATTCGCCAATGACAAGAC-3′ (Rmut);

*Hoxa6*, 5′-CCGTGTATGGGAGTCACGGGCGCA-3′ (F) and 5′-CGCTGGCCTGCGTGGAGTTGATGA-3′ (Rwt) and 5′-CGTGTTCGAATTCGCCAATGACAAGAC-3′ (Rmut);

*Hoxb6*, 5′-GCGCAAGCTCGACTGCGCACAG-3′ (F) and 5′-TCTTGCACGAATTCATGCGCTG-3′ (Rwt) and 5′-TTCAAGCCCAAGCTTTCGCGAG-3′ (Rmut);

*Hoxc6*, 5′-GTCGGTTACGGAGCGGACCGGAG-3′ (F) and 5′-CACAGAGCATTGGCGATCTCGATGC-3′ (Rwt) and 5′-CGTGTTCGAATTCGCCAATGACAAGAC-3′ (Rmut);

*Hoxa9*, 5′-GCTCGCTCCACTCGGAAGAA-3′ (F) and 5′-GGGAGATGAGGCCTGGGATT-3′ (Rwt) and 5′-TCTATCGCCTTCTTGACGAGTTC-3′ (Rmut);

*Hoxb9*, 5′-CTCCAATGCCAGGGGAGTAG-3′ (F) and 5′-CTTCTCTAGCTCCAGCGTCTGG-3′ (Rwt) and 5′-GTGTTCGAATTCGCCAATGACAAG-3′ (Rmut);

*Hoxc9*, 5′-GCAACCCCGTGGCCAACTGGATCC-3′ (F) and 5′-AAGACGGTGGGCTTTTCTCTATCTTGT-3′ (Rwt) and 5′-CGTTCATGAATATTCAGTTCACCGCTGA-3′ (Rmut);

*Hoxd9*, 5′-AGCGAACTGGATCCACGCTCGCTCCA-3′ (F) and 5′-GACTTGTCTCTCTGTAAGGTTCAGAAT-3′ (Rwt) and 5′-GTGTTCGAATTCGCCAATGACAAG-3′ (Rmut).

Genotyping for *Hox10* and *Hox11* mutants was as described previously (Wellik and Capecchi, 2003).

### In situ hybridization

In situ hybridization analyses were performed as described previously (Huppert et al., 2005; Wellik et al., 2002). The *Hoxd11* probe was previously published (Izpisua-Belmonte et al., 1991). The *Hoxb6* probe and the *Neo*$^{r}$ probe were generated by PCR. T3 sites were incorporated into the reverse primers, and the PCR product was used in an in vitro transcription reaction to produce DIG-labeled RNA probes. The following primers were used for probe generation (F, forward; R, reverse; T3 site underlined): *Neo*$^{r}$, 5′-GAAGGGACTGGCTGCTATTG-3′ (F) and 5′-GAGATTAACCCTCACTAAAGGGAAATATCACGGGTAGCCAACG-3′ (R); *Hoxb6*, 5′-GAGTCTGGGGACTTGCTGTC-3′ (F) and 5′-GAGATTAACCCTCACTAAAGGGATTCACGTCCGGAGCTAAGAC-3′ (R).

## RESULTS

Whole skeletal analyses of the *Hox5*, *Hox6* and *Hox9* paralogous mutants at E18.5 revealed patterning defects throughout the rib cage. *Hox5* and *Hox6* mutants were found to have shortened sternums and to be missing a complete first rib (Fig. 1A,B). In *Hox5* mutants, an eighth rib was attached to the sternum (Fig. 1A,E), and fusions were observed in the cervical vertebrae (Fig. 1A, black arrows). In *Hox9* quadruple mutants, the first rib formed but did not always attach to the sternum. Growth of the posterior ribs was abnormal and rib attachment to the sternum continued past T7 to T13 or ‘T14’. Additionally, four vertebrae posterior to T13 formed ribs (Fig. 1D and data not shown).

A ventral view of the intact rib cage (Fig. 1E-H) demonstrates the sternal defects in the three sets of mutants. *Hox5* mutants were missing the manubrium, and the second rib often fused with the third before attaching to the sternum (Fig. 1E). The clavicles were attached by connective tissue to the rib cage, but did not articulate with it directly (Fig. 1E, green asterisk). In the *Hox6* mutants, distal rib fusions were seen from T2 to T4, the sternabrae were poorly formed or missing, and the xiphoid process was reduced or absent (Fig. 1F, orange asterisk). *Hox9* mutants exhibited distal rib fusions of the anterior-most ribs, and extensive growth and fusion of extra posterior ribs to the sternum (Fig. 1H). Distinct sternabrae did not form. Rather, the sternum was ossified and mispatterned along its entire AP length. From views of the whole skeleton, defects were apparent throughout much of the rib cage in each set of mutants, but colinear defects were not immediately apparent.

Upon dissection and examination of individual vertebral elements, it was apparent that the somite-derived, primaxial skeletal defects occurred with distinct AP boundaries for each of the three sets of paralogous mutants. In *Hox5* mutants, C3 through T2 demonstrated anterior homeotic transformations (Fig. 2A). C3 through T1 in the *Hox5* mutants displayed characteristics normally associated with C2, the axis. Notably, the dorsal cartilage was thickened and formed a distinct curvature at the top of the vertebra (Fig. 2A, red arrows) and the rounded shape of the vertebral elements was maintained. The anterior projection that normally forms on T2 (Fig. 2A, green arrow) did not form completely, but appeared similar to controls by T3. The vertebral foramina extended beyond the normal posterior limit of C6 to C7 (Fig. 2A, black arrow) and ribs initiated but did not extend on T1 (100% penetrance).

By contrast, in the *Hox6* mutants, anterior homeotic transformations of the primaxial elements began at C6 and continued through T6 (Fig. 2B). C7 showed a continuation of the vertebral foramina as in the *Hox5* mutants (Fig. 2B, black arrow). T1, however, had no partial rib formation, appearing identical to C7 in controls (100% penetrance). The morphology of the first three thoracic vertebral bodies was similar to cervical vertebrae, and the anterior projection normally found on T2 was not apparent until T4 and continued through T6 (Fig. 2B, green arrows). Importantly, the posterior thoracic, lumbar and sacral skeletons were completely normal in appearance and position in both *Hox5* and *Hox6* paralogous mutants.

Primaxial defects in the *Hox9* quadruple mutants provided evidence of anterior homeotic transformations throughout the posterior thoracic skeleton and into the lumbar region (Fig. 2C). The morphology of T8 through L2 displayed transformations to a T7-like phenotype. By L5, the axial skeleton had resumed normal

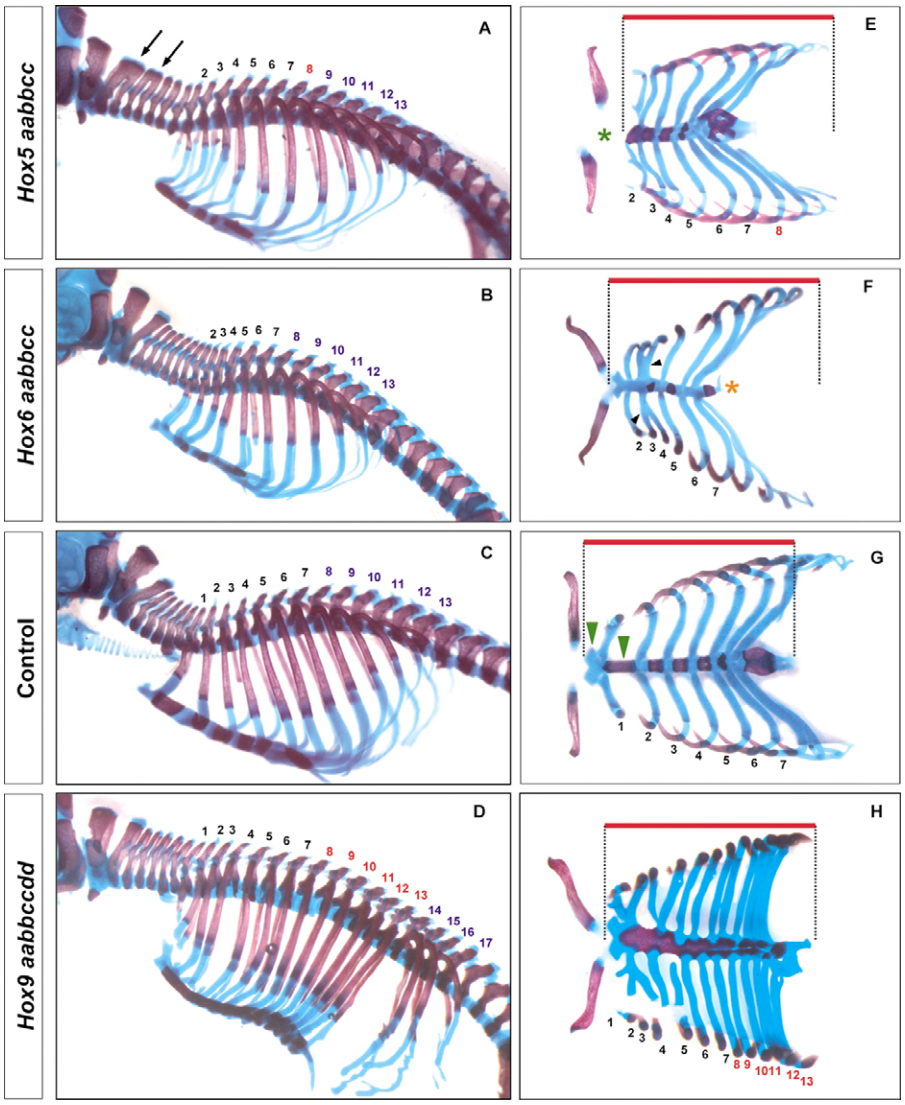


**Fig. 1. Whole skeletal phenotypes from *Hox5*, *Hox6* and *Hox9* paralogous mutant mice.** Lateral and ventral views of the rib cages of *Hox5* (**A**,**E**), *Hox6* (**B**,**F**), wild-type (**C**,**G**) and *Hox9* (**D**,**H**) paralogous mutant mice at E18.5. *Hox5* paralogous mutants refer to the genotype *Hoxa5*$^{-/-}$; *Hoxb5*$^{-/-}$; *Hoxc5*$^{-/-}$ (*Hox5aabbcc*), *Hox6* mutants refers to the genotype *Hoxa6*$^{-/-}$; *Hoxb6*$^{-/-}$; *Hoxc6*$^{-/-}$ (*Hox6aabbcc*), and *Hox9* paralogous mutants refers to the genotype *Hoxa9*$^{-/-}$; *Hoxb9*$^{-/-}$; *Hoxc9*$^{-/-}$; *Hoxd9*$^{-/-}$ (*Hox9aabbccdd*). In lateral views (A-D), all vertebrae having visible ribs are numbered, whereas in ventral views (E-H), only those that articulate with the sternum are numbered. The rib cages in E-H are intact (white paper inside the rib cage hides the dorsal aspects of the rib cages). The red bar in E-H provides a size reference for the length of the sternum. Black numbers indicate ribs that normally connect with the sternum, red numbers indicate extra ribs connecting to the sternum, and blue numbers indicate floating ribs. Arrows in A mark fused cervical vertebrae. Green asterisk in E marks connective tissue in place of missing manubrium and first sternabra. Orange asterisk in F denotes missing xiphoid process. Green arrowheads in G denote wild-type manubrium and first sternabra.

patterning. However, unlike other Hox paralogous mutants (*Hox5* and *Hox6* above, and *Hox7*, *Hox8*, *Hox10* and *Hox11*) (Chen et al., 1998; van den Akker et al., 2001; Wellik and Capecchi, 2003), the axial skeletons of the *Hox9* mutants posterior to the observed transformations were shifted caudally by two vertebral segments. The vertebra at the level of L5 in the *Hox9* mutants appeared indistinguishable from the L3 in controls, and normal patterning continued posterior to this element, but was offset by two vertebral elements (Fig. 2C). Dorsal views of whole skeletons show the shift of the axial skeleton posterior to the anterior homeotic transformations (Fig. 2D,E). Yellow stars indicate the normal position for L1 and L6. Note the posterior shift of the sacrum and thus displacement of pelvic attachment in the *Hox9* quadruple mutant. Nonetheless, the *Hox9* mutants had an average of two fewer caudal vertebrae than controls, so the total number of vertebrae formed was unchanged in these animals.

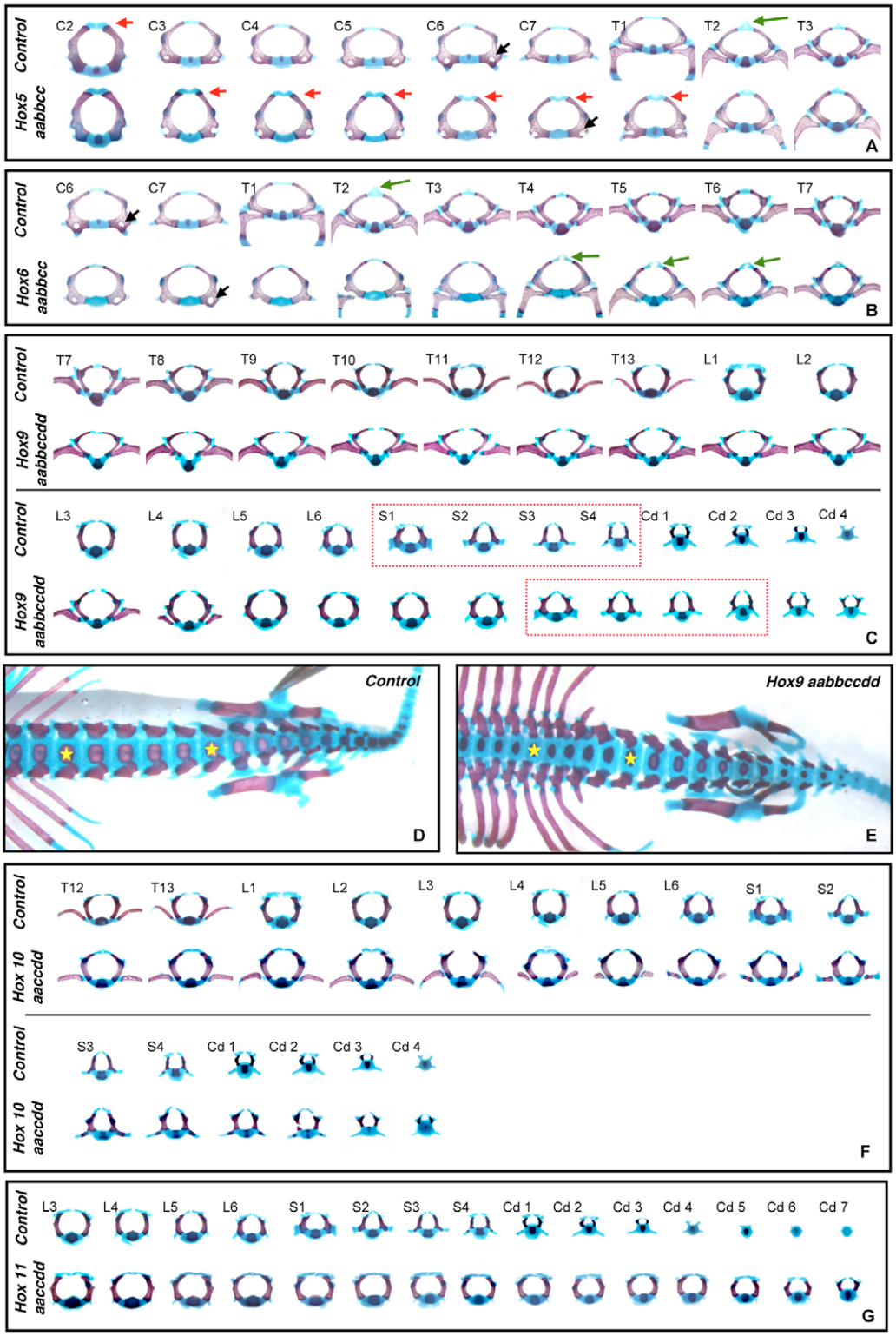


**Fig. 2. Anterior homeotic transformations of vertebral elements in *Hox5*, *Hox6*, *Hox9*, *Hox10* and *Hox11* paralogous mutants.** (**A-C**,**F**,**G**) Anterior views of individual vertebrae from controls (upper row) and mutants (lower row) for each set of paralogous mutants for *Hox5* (A), *Hox6* (B), *Hox9* (C), *Hox10* (F), *Hox11* (G). The position of each vertebra in controls is indicated by C (cervical), T (thoracic), L (lumbar), S (sacral) or Cd (caudal), followed by a number identifying its position in each region. Vertebral elements anterior and posterior to those shown in the figure appear identical to controls. (**D**,**E**) Dorsal views of control (D) and *Hox9* quadruple mutant (E) axial skeletons. In the control mouse, the sacrum is immediately caudal to six lumbar vertebrae (indicated by yellow stars on L1 and L6). In the *Hox9* mutant, the lumbar region is extended by two vertebral elements. The yellow stars in E mark control positions of the first and sixth lumbar vertebrae.

As the posterior region of the defects in the quadruple *Hox9* mutants demonstrates extra rib formation on the first four lumbar vertebrae, we compared the individual vertebral phenotypes of these animals with those from the *Hox10* triple mutants, which we previously reported to have rib formation on all lumbar vertebrae (Wellik and Capecchi, 2003). In *Hox10* triple mutants, rib formation was seen on all six lumbar vertebrae and even the sacral vertebrae showed conversion of the sacral lateral processes to rib-like outgrowths (Fig. 2F). However, the shape of the lumbar vertebral elements in the *Hox10* mutants appeared similar to lumbar vertebrae in controls, and the rib projections on all lumbar vertebrae in *Hox10* mutants were relatively small, much like the posterior-most thoracic vertebrae. By contrast, in *Hox9* quadruple mutants, the early lumbar elements with rib projections had vertebral bodies that appeared morphologically similar to more-anterior thoracic vertebrae and the rib projections on these elements were very long and also appeared similar to more-anterior thoracic vertebrae (Fig. 2, compare C with F). Thus, although the phenotype of rib outgrowth occurs in the first four lumbar vertebrae of both *Hox9* and *Hox10* paralogous mutants, these phenotypes are not identical, but rather represent phenotypes from different levels of the thoracic vertebrae.

Individual vertebral elements from the *Hox11* triple mutant animals allow a comparison of the overlapping sacral phenotypes between the *Hox10* mutants and *Hox11* mutants. Both mutants demonstrated clear phenotypes throughout the sacral region, but, whereas the *Hox10* mutants showed primarily a conversion of the normal lateral processes to those of a thoracic or rib-like character (Fig. 2F), the *Hox11* mutants showed a transformation of this entire region to a lumbar-like phenotype (Fig. 2G). Again, the morphological changes associated with the sacral vertebrae in these two sets of mutants are distinct.

*Hox5*, *Hox6* and *Hox9* mutants all have smaller rib cages than those in controls. As the size of the rib cage is a product of contributions from both the somite-derived, primaxial vertebral bodies and proximal ribs, as well as the lateral plate-derived, abaxial sternal skeleton, thoracic elements with the ribs intact were examined. In *Hox5* mutants (Fig. 3A, left column), T1 had incomplete rib projections and ribs from T2 extended but often did not reach the sternum (64%). Yet the primaxial vertebrae and rib angles were largely normal posterior to T1, suggesting that the smaller rib cage is due primarily to the severe defects in the lateral plate-derived sternum. By contrast, the *Hox6* mutants showed significant defects in the somite-derived, thoracic vertebral elements as well as in the sternum. Anterior homeotic transformations of the rib projections in the *Hox6* mutants extended from T2 through T6 (Fig. 3A, right column). Red arrows show that T2 through T4 have proximal rib angles similar to those of T1 in control skeletons. These defects, along with the severe defects in the lateral plate-derived sternal skeleton (Fig. 1B,F), result in the large decrease in the size of the rib cages in *Hox6* mutants.

The somite-derived vertebrae from the anterior thoracic skeleton (T1-T7) of the *Hox9* mutants were patterned normally, although fusions at the distal portion of the first three ribs were observed (Fig. 3B and Fig. 1H). Anterior homeotic transformations of the somite-derived skeleton were seen from T8 through L4. Unlike in the controls, ribs from T8 through T13 in *Hox9* mutants continued to grow distally and attach to the sternum, similar to more-anterior

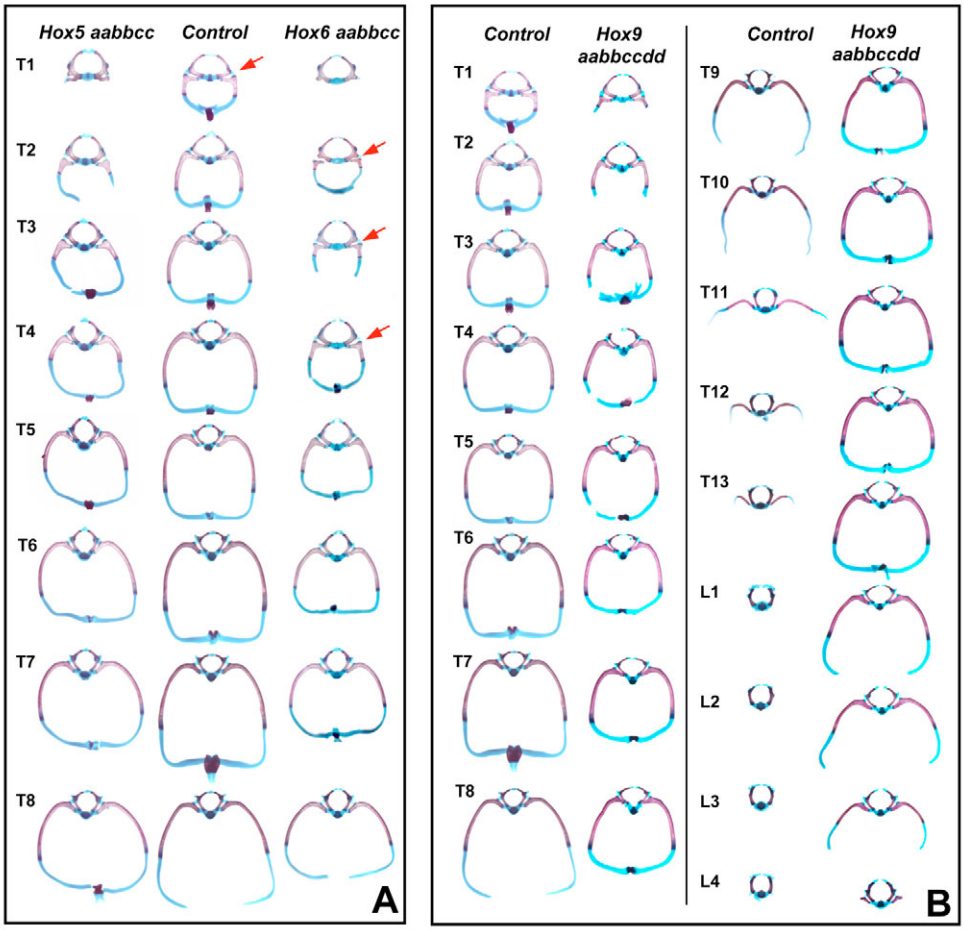


**Fig. 3. Rib and sternal abnormalities in the *Hox5*, *Hox6* and *Hox9* paralogous mutants.** (**A**) Individual skeletal elements, dissected with ribs attached, from the upper thoracic region of *Hox5* paralogous mutant, wild-type and *Hox6* paralogous mutant mice. The first column shows the first through eighth thoracic elements from a *Hox5* mutant mouse (the ventral ribs on T2 in this animal are incompletely formed). The second column depicts the same elements from a wild-type control mouse. The elements in the third column are from a *Hox6* mutant (in this mouse, T3 was fused with T4, and so appears incompletely formed). Red arrows denote the rib angle of control T1 and the phenotypic similarity in *Hox6* mutant T2 through T4. (**B**) Individual skeletal elements, with ribs attached, from the thoracic and lumbar regions of a *Hox9* paralogous mutant mouse (right column) are compared with those of a wild-type control (left column).

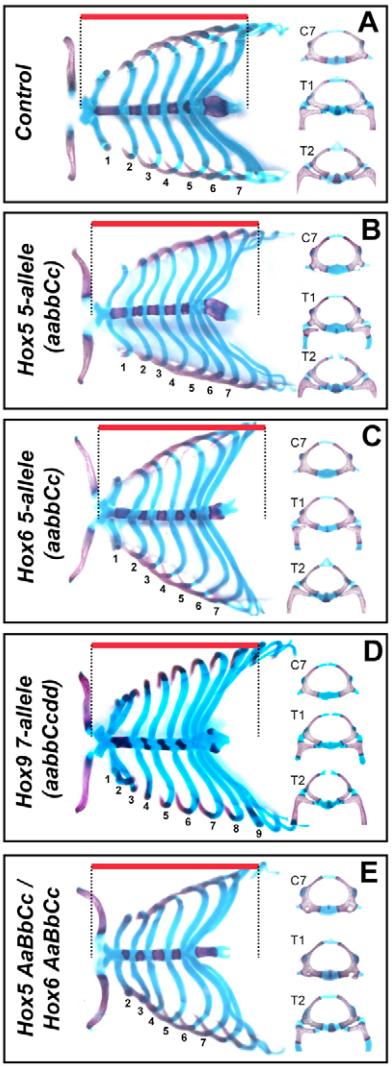


**Fig. 4. Defects in the rib cage of Hox mutant mice show functional redundancy.** Ventral views of the skeletal phenotypes from wild-type (**A**), *Hox5* five-allele (**B**), *Hox6* five-allele (**C**), *Hox9* seven-allele (**D**) and *Hox5*/*Hox6* trans-triple heterozygous (**E**) mice. Numbers below the rib cage indicate the thoracic vertebrae with ribs that fuse to the sternum. The red bar is included as a size reference. Note that any combination of five mutant alleles of *Hox5* or *Hox6* (Aabbcc, aaBbcc and aabbCc) shows very similar phenotypes to the ones shown in B and C. In the *Hox9* paralogous group, however, *Hoxc9* contributes more strongly to extra sternal rib growth and fusion than the other *Hox9* genes (data not shown).

vertebrae (Fig. 3B). Despite many extra fused ribs, the rib cage was smaller than in controls owing to apparent growth constraints from crowding at the sternum.

Redundancy continues to play a key role in understanding Hox function. *Hox5* and *Hox6* mutants possessing any combination of five of the possible six mutant alleles were much less affected than the paralogous mutants (Fig. 4A-C). Similarly, the seven-allele *Hox9* mutant in Fig. 4D has a much less severe phenotype, with only two extra ribbed vertebrae, T8 and T9, attached to the sternum.

Because of the overlap in phenotypes between the *Hox5* and *Hox6* paralogous mutants, we generated trans-triple heterozygous embryos (*5AaBbCc/6AaBbCc*) to examine whether *Hox5* and *Hox6* paralogous groups are functionally equivalent in their respective patterning roles. Trans-triple heterozygotes were found to have a less severe phenotype than either *Hox5* or *Hox6* triple mutants in both the primaxial and abaxial skeleton despite containing the same number of mutant alleles (Fig. 4A,E), demonstrating that the two paralogous groups do not function redundantly in axial patterning.

Phenotypes in overlapping regions of adjacent paralogous mutants are distinct from one another in all of the cases we have examined to date, suggesting that the phenotypes are not due to changes in the expression of more-posterior Hox paralogous genes. To test for this possibility, we performed in situ hybridization to determine whether the anterior limit of expression of the next-most posterior group Hox genes are perturbed in Hox paralogous mutants. In *Hox5* triple mutants, the expression of *Hoxb6* was observed at the same anterior limit as in controls at E11.5 (Fig. 5A,B). Similarly, in more-posterior regions of the embryo, the anterior limit of *Hoxd11* expression in *Hox10* triple mutants was unchanged compared with controls (Fig. 5C,D). These data support the conclusion that adjacent Hox paralogous genes are co-expressed and have distinct functions in overlapping AP regions.

Furthermore, the rib cage phenotypes of the *Hox5*, *Hox6* and *Hox9* paralogous mutants demonstrate differential phenotypic boundaries for the somite-derived vertebral elements and the lateral plate-derived sternum. The genetic results suggest that expression and function in the somites might be distinct from expression and function in the lateral plate mesoderm. To ascertain whether expression levels correlate with the genetic results, we examined the expression pattern of these paralogous group genes at several developmental stages. We found that Hox expression is dynamic during early developmental time points, particularly in the lateral plate. The anterior expression boundary in the somites of the *Hox5* paralogous group genes appeared to be at approximately the level of the ninth developing somite at E9.5 (Fig. 5E, white arrow), with the lateral plate expression limit slightly anterior to this, including in the early limb bud (Fig. 5E, black arrow). By E10.5, somite staining could be visualized more anteriorly, with the expression limit at somite five (Fig. 5F, white arrow). Lateral plate staining could still be seen along the entire lateral plate anterior to the forelimb and between the forelimb and hindlimb, consistent with sternal defects throughout the AP length of the sternum (Fig. 5F). By E12.5, intense staining in the somite could be detected up to an anterior limit at somite 6/7 (Fig. 5G, white arrow), although fainter staining could be detected in two anterior somites. This expression in somites correlates with the observed genetic phenotypes beginning at C3, and is also in complete agreement with reports of *Hoxa5*, *Hoxb5* and *Hoxc5* somite expression boundaries, which were examined previously at the later time point (Burke et al., 1995; Gaunt et al., 1990). Lateral plate expression cannot be clearly detected after E11.5. It cannot be discerned whether expression of these genes is absent or has fallen to very low levels.

The anterior limits of somitic expression for *Hox6* appeared to be more similar in all of the stages examined, approximately at the somite 12 boundary (Fig. 5H-J, white arrows). This is consistent with previous reports for these genes at E12.5 and E13.5 (Burke et al., 1995; Kostic and Capecchi, 1994; Toth et al., 1987), and also with the genetic phenotypes reported here which begin at C6. Lateral plate expression was visible from the forelimb area to more-posterior regions through E10.5 (Fig. 5H,I, black arrows), but expression was seen to decrease below background at later developmental stages, similar to the observation for the *Hox5* genes. This suggests that the contribution from *Hox5* and *Hox6* genes to

patterning the sternum is an early developmental event, but functionally significant expression levels that are too low to detect cannot be ruled out without conditional functional analyses.

The expression profile of *Hox9* during these developmental time points differs significantly from *Hox5* and *Hox6*. At E9.5, expression was intense in the tailbud and became fainter more anteriorly, with no clearly established anterior boundary. Expression in the lateral plate mesoderm reached levels just posterior to the developing heart (Fig. 5K, black arrow). By E10.5, a boundary at somite 23 could be seen in the paraxial mesoderm (white arrow), but the lateral plate expression remained intense far anterior to this, in the entire region between the forelimbs and hindlimbs (Fig. 5L, black arrow). The somitic boundary at somite 23 became even sharper by E11.5, in agreement with previous reports on these genes (Fig. 5M, white arrow) (Burke et al., 1995; Chen and Capecchi, 1997; Duboule and Dolle, 1989; Erselius et al., 1990); *Hoxd9* has been reported to have more-posterior somitic boundaries, but this would be masked by more-anterior expression of the remaining three paralogs (Burke et al., 1995; Duboule and Dolle, 1989). Unlike *Hox5* and *Hox6*, strong *Hox9* expression persisted in the lateral plate at this and later stages (Fig. 5M and data not shown). This expression pattern is consistent with the possibility that later expression in the lateral plate is important for *Hox9*-mediated repression of growth and attachment of posterior ribs to the sternum. Consistent with this, the anterior-most somitic boundary of *Hox9* expression is at somite levels well below that of the thoracic skeleton where distal rib phenotypes occur, with the exception of E9.5 during early boundary formation (Fig. 5K) (Burke et al., 1995; Chen and Capecchi, 1997). Clearly, conditional genetic analyses will be required to understand the contributions to sternal phenotype.

## DISCUSSION

Comparison of the phenotypes in the paralogous mutant groups (Fig. 6) leads to several important conclusions about the nature of the Hox code in vertebrate axial patterning. First, loss of paralogous Hox function consistently exhibits functional redundancy among Hox paralogous genes, and all paralogous mutant phenotypes in the primaxial skeleton can be clearly categorized as anterior homeotic transformations. As previously shown for the *Hox10* and *Hox11* paralogous genes, leaving just one wild-type allele in the absence of five alleles (in the case of *Hox5*, *Hox6*, *Hox10* and *Hox11*) or seven alleles (in the case of the *Hox9* genes) results in a less severe phenotype than removing all functional copies in a given paralogous group. Furthermore, these phenotypes show clear colinearity with more anteriorly expressed Hox genes affecting more-anterior regions of the somite-derived axial skeleton and more-posterior Hox genes affecting increasingly posterior regions.

Although anterior homeotic transformations in each paralogous mutant have distinct AP boundaries, the vertebrae that exhibit transformations in adjacent paralogous mutant groups significantly

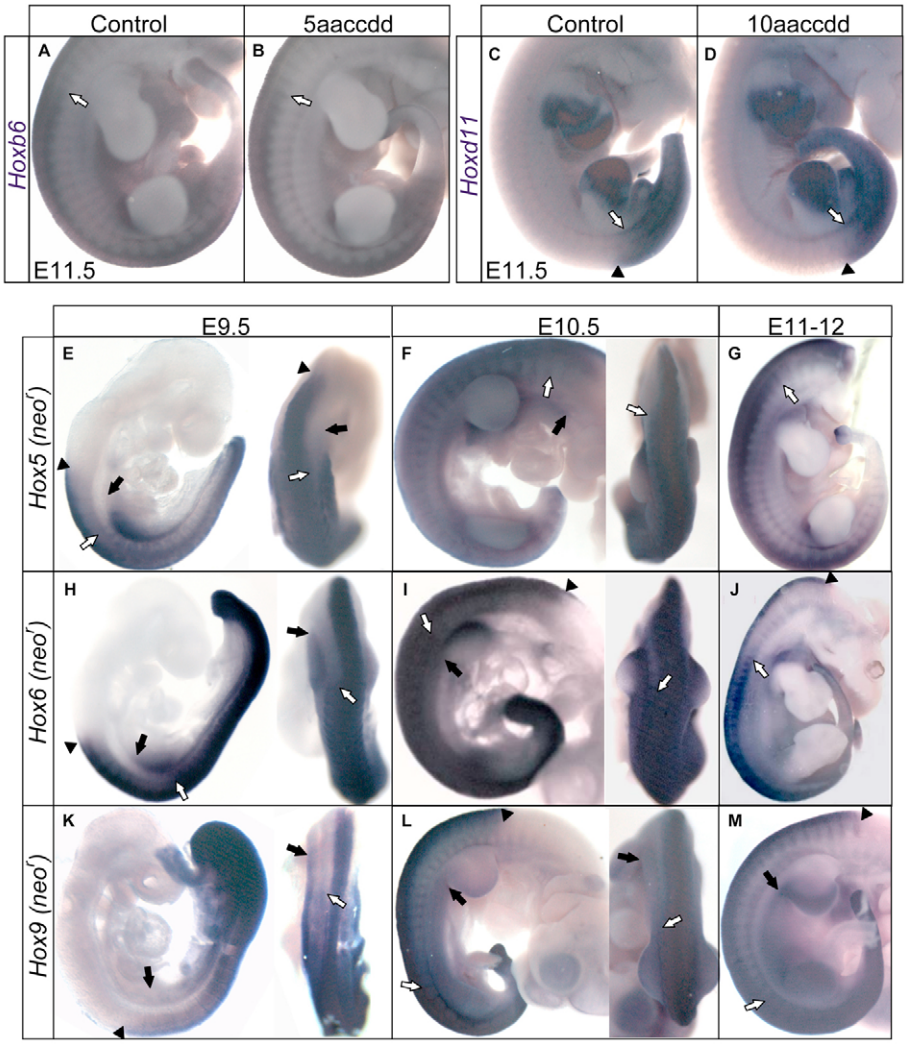


**Fig. 5. Hox expression during axial patterning.** The anterior boundary of *Hoxb6* expression at E11.5 is the same in control (**A**) and *Hox5* paralogous mutant (**B**) mice. The anterior boundary of *Hoxd11* expression in control (**C**) and *Hox10* paralogous mutants (**D**) is also equivalent. (**E-M**) A *Neo*$^{r}$ probe was used to demonstrate the anterior expression boundaries of the entire paralogous group in triple heterozygous animals (in the case of *Hox5* and *Hox6* embryos) or quadruple heterozygous mutants (for *Hox9* embryos), none of which have a phenotype. Each mutant allele has *Neo*$^{r}$ inserted into the Hox coding sequence. Somite anterior expression limits are marked with a white arrow and lateral plate anterior expression limits are marked with a black arrow. (The anterior expression limit for the neural tube, marked with a black arrowhead, is often far anterior to the somite expression boundary as published for the individual Hox genes referenced in the text.) E,F,H,I,K,L, embryos shown in lateral and dorsal view; G,J,M, embryos shown in lateral view only.

overlap (Fig. 6, red-shading indicates the AP region demonstrating anterior homeotic transformations; overlapping phenotypic regions between adjacent paralogous mutants are highlighted in yellow). Within the overlapping affected regions in adjacent paralogous mutants, however, the observed phenotypes are distinct, suggesting that each Hox paralogous group imparts unique morphological characteristics to the vertebrae. For example, whole skeletons of both *Hox5* and *Hox6* mutants each appear to be missing the first rib. However, inspection of the T1 element shows that *Hox5* mutants have transformations of the dorsal aspects of this element towards a C2 fate with small ribs initiating with complete penetrance (12 of 12, Fig. 2A). T1 from *Hox6* mutants, by contrast, show an anterior transformation to a C7 phenotype, with no likeness to C2 and no indication of rib initiation (11 of 11, Fig. 2B). In another example, both *Hox10* and *Hox11* paralogous mutants display phenotypes in all sacral vertebrae. Whereas loss of *Hox10* function results in a conversion of the sacral lateral wings to rib-like projections that fuse laterally, loss of *Hox11* results in transformation of sacral vertebrae to a lumbar-like morphology with no sacral wing projections and no lateral fusions (Fig. 2F,G) (Wellik and Capecchi, 2003). We also show that removal of the function of an entire paralogous group does not significantly affect the expression of the next-most posterior group of genes (Fig. 5A-D).

The current data strongly support the idea that the genetic function of each of the paralogous groups of Hox genes in axial patterning is distinct, and that the 'Hox code' is a combination of the unique morphological contributions imparted by each of the two or more paralogous groups functioning in a given AP region. These data are not in simple agreement with the posterior prevalence model, which has held that the patterning information at a given AP region relies on a single Hox gene or paralogous group (Kmita and Duboule, 2003) and that patterning information, in the case of overlapping expression of two or more Hox genes (or paralogous groups), is provided by the more posteriorly acting gene(s) (Duboule, 1991; Duboule and Morata, 1994). However, it is also clear from these genetic experiments that the morphology of the axial skeleton regains wild-type patterns posterior to the affected region. Therefore, not all of the Hox genes expressed in the posterior region of the early, developing embryo appear to function in axial patterning. As little or no information exists regarding when or how Hox genes function at a mechanistic level to impart vertebral morphologies, the significance of the early, nested Hox expression pattern is not clear. Unequivocal experiments to test the molecular nature of the 'Hox code' and the model of posterior prevalence await the discovery of confirmed downstream targets in Hox-regulated axial patterning, knowledge of when Hox-regulated axial patterning is imparted during embryogenesis, and details of Hox protein expression during crucial axial patterning events.

This study also demonstrates that Hox genes are crucial for patterning the lateral plate-derived, abaxial skeleton (the sternum and sternal ribs), that Hox gene function in the abaxial skeleton is independent of somite-derived patterning, and that this patterning is

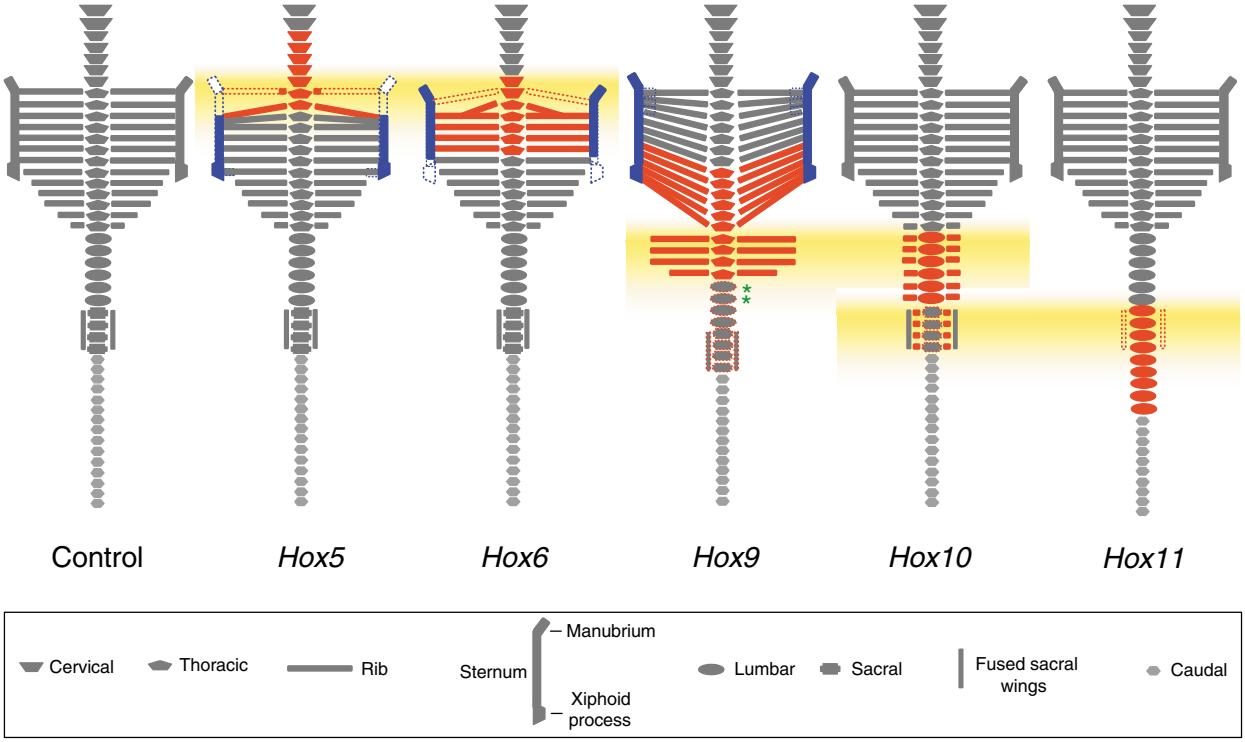


**Fig. 6. Schematic representation of paralogous Hox axial skeleton phenotypes.** Somite-derived, primaxial skeletal elements that exhibit anterior homeotic transformations in paralogous mutants are in red. Lateral plate-derived structures affected in paralogous mutants are in blue. Note that *Hox5*, *Hox6* and *Hox9* mutant phenotypes are offset in their AP extent for defects in the somite-derived (red) and lateral plate-derived (blue) skeleton. The yellow shading highlights somite-derived AP regions that are affected in adjacent paralogous mutant groups. In each case, the overlapping regions of phenotype display distinct vertebral morphologies for each paralogous mutant. The green asterisks in the *Hox9* mutant reflect the posterior shift of the axial skeleton. Mice normally possess 28-30 caudal vertebrae. Only 15 are represented here for simplicity. Despite changes in the number of caudal vertebrae in *Hox9* and *Hox11* paralogous mutants, the same average total numbers of vertebrae are present in all of the paralogous mutants depicted in this diagram, and are the same as in control animals.

not colinear. Formation of the manubrium appears to be uniquely a *Hox5*-regulated process (Fig. 1E). However, the *Hox5*, *Hox6* and *Hox9* mutants all have patterning defects along the AP length of the sternum, inconsistent with a strictly colinear contribution to patterning this lateral plate-derived structure (Fig. 6, blue-shaded abaxial defects). Furthermore, defects are found with complete penetrance in first rib and sternabra formation in *Hox5*, *Hox6* and *Hox9* paralogous mutants, *Hox5/Hox6* trans-triple heterozygotes, and *Hox7* and *Hox8* paralogous mutants (Chen et al., 1998; van den Akker et al., 2001), as well as with incomplete penetrance in many of the *Hox5* through *Hox9* single mutant animals and *Hoxb5/Hoxb6* trans-heterozygotes (Chen and Capecchi, 1997; Garcia-Gasca and Spyropoulos, 2000; Kostic and Capecchi, 1994; Rancourt et al., 1995). Taken together, the growth and formation of the first rib and sternabra is particularly sensitive to loss of *Hox5* through *Hox9* function. This phenotype is likely to be due to patterning disruptions in the lateral plate mesoderm that do not obey the colinear contribution to patterning that is clear in the somite-derived skeleton. A detailed understanding of Hox gene function in patterning the lateral plate-derived portion of the thoracic skeleton will require conditional analyses that can distinguish between the patterning contributions from these two distinct tissues in the development of the rib cage.

The combined genetic data on Hox paralogous phenotypes in the axial skeleton clearly demonstrate that Hox genes do not contribute to the total number of vertebral elements formed. Combined results from the *Hox4* triple mutants and the *Hox5* through *Hox11* paralogous mutants (Chen et al., 1998; van den Akker et al., 2001; Wellik and Capecchi, 2003) (this report) demonstrate that although the morphology of AP-restricted regions display defects throughout the axial skeleton, the number of elements do not change.

In conclusion, the data reported here contribute significantly to our genetic understanding of Hox function in vertebrate axial patterning. Loss of Hox paralogous function results in anterior homeotic transformations throughout the somite-derived axial skeleton, including the thoracic skeleton. The lateral plate-derived skeleton appears to be patterned independently from the somite-derived skeleton and lateral plate axial patterning is not colinear. By establishing that consistent genetic mechanisms operate in vertebrate axial patterning, this framework will hopefully allow us to examine in detail the molecular function of Hox genes in this system.

We thank J. Fallon, A. Boulet and B. Bisgrove for critically reviewing previous versions of the manuscript. This work was supported in part by Research Grant No. 5-FY05-48 from the March of Dimes Birth Defects Foundation and by a University of Michigan Organogenesis Predoctoral Fellowship Award, T32-HD007505 (A.R.Y.).

**References**

**Bachiller, D., Macias, A., Duboule, D. and Morata, G.** (1994). Conservation of a functional hierarchy between mammalian and insect Hox/HOM genes. *EMBO J.* **13**, 1930-1941.
**Boulet, A. M. and Capecchi, M. R.** (1996). Targeted disruption of *hoxc-4* causes esophageal defects and vertebral transformations. *Dev. Biol.* **177**, 232-249.
**Burke, A. C. and Nowicki, J. L.** (2003). A new view of patterning domains in the vertebrate mesoderm. *Dev. Cell* **4**, 159-165.
**Burke, A. C., Nelson, C. E., Morgan, B. A. and Tabin, C.** (1995). Hox genes and the evolution of vertebrate axial morphology. *Development* **121**, 333-346.
**Chen, F. and Capecchi, M. R.** (1997). Targeted mutations in hoxa-9 and hoxb-9 reveal synergistic interactions. *Dev. Biol.* **181**, 186-196.
**Chen, F. and Capecchi, M. R.** (1999). Paralogous mouse *Hox* genes, *Hoxa9*, *Hoxb9*, and *Hoxd9*, function together to control development of the mammary gland in response to pregnancy. *Proc. Natl. Acad. Sci. USA* **96**, 541-546.
**Chen, F., Greer, J. and Capecchi, M. R.** (1998). Analysis of *Hoxa7/Hoxb7* mutants suggests periodicity in the generation of the different sets of vertebrae. *Mech. Dev.* **77**, 49-57.
**Colberg-Poley, A. M., Voss, S. D., Chowdhury, K., Stewart, C. L., Wagner, E. F. and Gruss, P.** (1985). Clustered homeo boxes are differentially expressed during murine development. *Cell* **43**, 39-45.
**Davis, A. P., Witte, D. P., Hsieh-Li, H. M., Potter, S. S. and Capecchi, M. R.** (1995). Absence of radius and ulna in mice lacking *hoxa-11* and *hoxd-11*. *Nature* **375**, 791-795.
**Duboule, D.** (1991). Patterning in the vertebrate limb. *Curr. Opin. Genet. Dev.* **1**, 211-216.
**Duboule, D. and Dolle, P.** (1989). The structural and functional organization of the murine HOX gene family resembles that of Drosophila homeotic genes. *EMBO J.* **8**, 1497-1505.
**Duboule, D. and Morata, G.** (1994). Colinearity and functional hierarchy among genes of the homeotic complexes. *Trends Genet.* **10**, 358-364.
**Erselius, J. R., Goulding, M. D. and Gruss, P.** (1990). Structure and expression pattern of the murine Hox-3.2 gene. *Development* **110**, 629-642.
**Garcia-Gasca, A. and Spyropoulos, D. D.** (2000). Differential mammary morphogenesis along the anteroposterior axis in Hoxc6 gene targeted mice. *Dev. Dyn.* **219**, 261-276.
**Gaunt, S. J., Coletta, P. L., Pravtcheva, D. and Sharpe, P. T.** (1990). Mouse Hox-3.4: homeobox sequence and embryonic expression patterns compared with other members of the Hox gene network. *Development* **109**, 329-339.
**Greer, J., Puetz, J., Thomas, K. R. and Capecchi, M. R.** (2000). Maintenance of functional equivalence during paralogous Hox gene evolution. *Nature* **403**, 661-665.
**Gruss, P. and Kessel, M.** (1991). Axial specification in higher vertebrates. *Curr. Opin. Genet. Dev.* **1**, 204-210.
**Horan, G. S. B., Ramirez-Solis, R., Featherstone, M. S., Wolgemuth, D. J., Bradley, A. and Behringer, R. R.** (1995). Compound mutants for the paralogous *hoxa-4*, *hoxb-4*, and *hoxd-4* genes show more complete homeotic transformations and a dose-dependent increase in the number of vertebrae transformed. *Genes Dev.* **9**, 1667-1677.
**Huppert, S. S., Ilagan, M. X., De Strooper, B. and Kopan, R.** (2005). Analysis of Notch function in presomitic mesoderm suggests a gamma-secretase-independent role for presinilins in somite differentiation. *Dev. Cell* **8**, 677-688.
**Izpisua-Belmonte, J. C., Falkenstein, H., Dolle, P., Renucci, A. and Duboule, D.** (1991). Murine genes related to the Drosophila AbdB homeotic genes are sequentially expressed during development of the posterior part of the body. *EMBO J.* **10**, 2279-2289.
**Jeannotte, L., Lemieux, M., Charron, J., Poirier, F. and Robertson, E. J.** (1993). Specification of axial identity in the mouse: role of the Hoxa-5 (Hox1.3) gene. *Genes Dev.* **7**, 2085-2096.
**Kessel, M. and Gruss, P.** (1990). Murine developmental control genes. *Science* **249**, 374-379.
**Kessel, M. and Gruss, P.** (1991). Homeotic transformations of murine vertebrae and concomitant alteration of the Hox code induced by retinoic acid. *Cell* **67**, 89-104.
**Kmita, M. and Duboule, D.** (2003). Organizing axes in time and space; 25 years of colinear tinkering. *Science* **301**, 331-333.
**Kostic, D. and Capecchi, M. R.** (1994). Targeted disruptions of the murine Hoxa-4 and Hoxa-6 genes result in homeotic transformations of components of the vertebral column. *Mech. Dev.* **46**, 231-247.
**Lewis, E. B.** (1963). Genes and developmental pathways. *Am. Zool.* **3**, 33-56.
**Lewis, E. B.** (1978). A gene complex controlling segmentation in *Drosophila*. *Nature* **276**, 565-570.
**Nowicki, J. L. and Burke, A. C.** (2000). *Hox* genes and morphological identity: axial patterning versus lateral patterning in the vertebrate mesoderm. *Development* **127**, 4265-4275.
**Nowicki, J. L., Takimoto, R. and Burke, A. C.** (2003). The lateral somitic frontier: dorso-ventral aspects of anterio-posterior regionalization in avian embryos. *Mech. Dev.* **120**, 227-240.
**Patterson, L. T., Pembaur, M. and Potter, S. S.** (2001). *Hoxa11* and *Hoxd11* regulate branching morphogenesis of the ureteric bud in the developing kidney. *Development* **128**, 2153-2161.
**Rancourt, D. E., Tsuzuki, T. and Capecchi, M. R.** (1995). Genetic interaction between hoxb-5 and hoxb-6 is revealed by nonallelic noncomplementation. *Genes Dev.* **9**, 108-122.
**Rossel, M. and Capecchi, M. R.** (1999). Mice mutant for both *Hoxa1* and *Hoxb1* show extensive remodeling of the hindbrain and defects in craniofacial development. *Development* **126**, 5027-5040.
**Toth, L. E., Slawin, K. L., Pintar, J. E. and Nguyen-Huu, M. C.** (1987). Region-specific expression of mouse homeobox genes in the embryonic mesoderm and central nervous system. *Proc. Natl. Acad. Sci. USA* **84**, 6790-6794.
**van den Akker, E., Fromental-Ramain, C., de Graaff, W., Mouellic, H. L., Brulet, P., Chambon, P. and Deschamps, J.** (2001). Axial skeletal patterning in mice lacking all paralogous group 8 Hox genes. *Development* **128**, 1911-1921.
**Wahba, G. M., Hostikka, S. L. and Carpenter, E. M.** (2001). The paralogous *Hox* Genes *Hoxa10* and *Hoxd10* interact to pattern the mouse hindlimb peripheral nervous system and skeleton. *Dev. Biol.* **231**, 87-102.
**Wellik, D. M. and Capecchi, M. R.** (2003). *Hox10* and *Hox11* genes are required to globally pattern the mammalian skeleton. *Science* **301**, 363-366.
**Wellik, D. M., Hawkes, P. J. and Capecchi, M. R.** (2002). *Hox11* paralogous genes are essential for metanephric kidney induction. *Genes Dev.* **16**, 1423-1432.